Journal of Colloid and Interface Science 388 (2012) 144–150

Contents lists available at SciVerse ScienceDirect

Journal of Colloid and Interface Science

www.elsevier.com/locate/jcis

High ethanol sensitivity of Palladium/TiO_2 nanobelt surface heterostructures dominated by enlarged surface area and nano-Schottky junctions

Dongzhou Wang [a], Weijia Zhou [a], Peiguang Hu [a], Yu Guan [b], Limei Chen [a], Jianhua Li [a], Guancong Wang [a], Hong Liu [a,*], Jiyang Wang [a], Guozhong Cao [c,1], Huaidong Jiang [a]

[a] *State Key Laboratory of Crystal Materials, Center of Bio & Micro/Nano Functional Materials, Shandong University, 27 Shandanan Road, Jinan 250100, PR China*
[b] *School of Chemistry and Chemical Engineering, Shandong University, 27 Shandanan Road, Jinan 250100, PR China*
[c] *Department of Materials Science and Engineering, University of Washington, Seattle, WA 98195, USA*

ARTICLE INFO

Article history:
Received 12 July 2012
Accepted 18 August 2012
Available online 28 August 2012

Keywords:
Hydrothermal method
Surface-coarsening
Pd nanoparticle
TiO_2 nanobelt surface heterostructure
Gas sensors

ABSTRACT

TiO_2 nanobelts were prepared by the hydrothermal growth method. The surface of the nanobelts was coarsened by selective acid corrosion and functionalized with Pd catalyst particles. Three nanobelt samples (TiO_2 nanobelts, surface-coarsened TiO_2 nanobelts and Pd nanoparticle/TiO_2 nanobelt surface heterostructures) were configured as gas sensors and their sensing ability was measured. Both the surface-coarsened nanobelts and the Pd nanoparticle-decorated TiO_2 nanobelts exhibited dramatically improved sensitivity to ethanol vapor. Pd nanoparticle-decorated TiO_2 nanobelts with surface heterostructures exhibited the best sensitivity, selectivity, working temperature, response/recovery time, and reproducibility. The excellent ethanol sensing performance is attributed to the large surface area and enhancement by Schottky barrier-type junctions between the Pd nanoparticles and TiO_2 nanobelts.

1. Introduction

As a wide band gap semiconductor, titanium dioxide (TiO_2) has wide applications in photocatalysis [1–3], lithium-ion batteries [4,5], chemical and bio-sensors [6,7], hydrogen production and storage [8,9], sensitized or hybrid solar cells [10,11], and biomedicine [12]. Recently, one-dimensional single-crystalline TiO_2 (in the form of nanotubes, nanobelts, nanowires, and nanorods) has received much attention due to a combination of favorable mass and charge transport properties and large specific surface area. In comparison with TiO_2 nanoparticles, one-dimensional TiO_2 nanostructures exhibit a high surface-to-volume ratio, favorable pathways for electron and hole transport, a stable configuration and ease of maneuverability [13].

TiO_2 nanomaterials have been widely used as sensors in many fields, such as the biomedical, chemical, environmental, and food industries [14–18]. Therefore, a great deal of effort has been spent in investigating and developing TiO_2-based gas sensors. Previous studies have reported on sensors made with TiO_2 films, a typical 2-D nanostructure [19–26]. However, the performance of those TiO_2-based sensors was limited by several drawbacks, including low sensitivity, high working temperature, poor selectivity, and long response/recovery time. In order to improve the sensitivity, selectivity, working temperature, and response/recovery time, several methods have been explored, such as using doped TiO_2 [27–32], functionalization with metal nanoparticles [14,26,33,34], and synthesis of different TiO_2 nanostructures [14,18,23,35,36]. Among these studies, 1-D nanostructured-TiO_2 has attracted more attention due to its large surface-to-volume ratio [14–16,18,34]. In addition, by assembling a variety of noble metal quantum dots and semiconductor nanostructures on the surface of one-dimensional TiO_2 nanomaterials, the sensing properties can be greatly enhanced. In our earlier work, the performance in the detection of ethanol by TiO_2 nanobelts, surface-coarsened TiO_2 nanobelts and surface-coarsened Ag-TiO_2 nanobelts was examined, and the results show obvious improvement over traditional TiO_2 thin films [14].

Limited research on the Pd nanoparticle-enhanced gas sensing properties of 1-D nanostructures has been published, such as on Pd–SnO nanowires [34] and Pd-carbon nanotubes [37]. Although both of these new materials possess improved sensitivity, their response and recovery time is too long for practical applications. The response and recovery time of Pd–SnO nanowires is about 50 s, and that of Pd-carbon nanotubes is 40 min. As we reported in a previous paper, TiO_2 nanobelts possess a very short response and recovery time of only 3–4 s. Compared with Ag nanoparticle/TiO_2 nanobelt heterostructures, the sensor based on Pd/TiO_2 nanobelt

---

* Corresponding author. Fax: +86 531 88362807.
E-mail addresses: hongliu@sdu.edu.cn (H. Liu), gzcao@u.washington.edu (G. Cao).
[1] Fax: +1 206 543 3100.

0021-9797/$ - see front matter © 2012 Elsevier Inc. All rights reserved.
http://dx.doi.org/10.1016/j.jcis.2012.08.034

heterostructure possesses many advantages, such as Pd/TiO_2 nanobelt heterostructure more stable and reliable than Ag/TiO_2 nanoheterostructure, because Pd nanoparticle is very difficult to be oxidized in air; the distribution and size of Pd nanoparticles on the nanobelts are easy to be controlled during the synthesis process, and then easy to be scaled up, the small size of Pd nanoparticles brings high sensitivity of the sensor; Pd/TiO_2 nanobelt heterostructures possesses much higher selectivity for detection of ethanol, which is one of the most important properties of a practicable gas sensor. It is surmised that assembling Pd nanoparticles on the surface of TiO_2 nanobelts will produce a high performance gas sensor material with high sensitivity, low response time, and most likely high selectivity.

In this paper, TiO_2 nanobelts and surface-coarsened TiO_2 nanobelts synthesized through a hydrothermal process were used as basic materials for constructing a gas sensor. Pd nanoparticles were synthesized and directly assembled on the surface of the TiO_2 nanobelts by a precipitation-reduction method to form a Pd nanoparticle/TiO_2 nanobelt heterostructure with accompanying enhancement of gas sensor properties. The sensitivity to ethanol vapor, carbon monoxide (CO), hydrogen (H_2), methane (CH_4), and acetone (CH_3COCH_3) was measured to evaluate the degree of sensitivity and gas selectivity. The results show that sensors consisting of Pd nanoparticle/TiO_2 nanobelt surface heterostructures (abbreviated as Pd NP/TiO_2 NB surface heterostructures) possess very high ethanol sensitivity, significantly short response-recovery time, low detection limit, and favorable selectivity. Because this material is easy to scale up, it could provide a practical route for the fabrication of low-cost high performance ethanol sensors.

2. Experimental section

The raw materials used in this work include titania P-25 (TiO_2; ca. 80% anatase, and 20% rutile), sodium hydroxide (NaOH), hydrochloric acid (HCl), sulfuric acid (H_2SO_4), sodium borohydride ($NaBH_4$), and palladium chloride ($PdCl_2$). They were purchased from the China National Medicines Corporation, Ltd. without further purification or other treatment.

TiO_2 nanobelts were prepared via an alkali hydrothermal process with titania P-25 as the raw material. The synthetic procedure has been reported in Refs. [14,38]. In a typical reaction, 0.1 g of P-25 powder was separated and dispersed into 20 mL of 10 M NaOH aqueous solution. After magnetically stirring for 10 min, the mixed solution was transferred into a Teflon-lined stainless steel autoclave, heated at 200 °C for 72 h, and then air-cooled to room temperature. The product was filtered and washed thoroughly with deionized water. The wet powder was immersed in 500 mL of 0.1 mol/L HCl aqueous solution at room temperature for 24 h and then washed thoroughly with deionized water to obtain $H_2Ti_3O_7$ nanobelts. The $H_2Ti_3O_7$ nanobelts were annealed at 600 °C for 3 h, and the ultimate product consisted of TiO_2 nanobelts.

Surface-coarsened TiO_2 nanobelts were prepared via an acid-assisted hydrothermal process as described in our early publications [14,38]. Briefly, 0.15 g of $H_2Ti_3O_7$ was separated into 20 mL of 0.02 M H_2SO_4 aqueous solution. After magnetically stirring for 10 min, the mixed solution was transferred into a Teflon-lined stainless steel autoclave, heated at 110 °C for 12 h, and then air-cooled to room temperature. The product was filtered and washed thoroughly with deionized water, annealed at 600 °C for 3 h, and the ultimate product consisted of surface-coarsened TiO_2 nanobelts.

The synthesis process of Pd NP/TiO_2 NB surface heterostructures (4 wt.% Pd) is described as follows. A quantity of 0.05 g of surface coarsened TiO_2 nanobelts and 2.56 mL of 1 g/L $PdCl_2$ deionized water solution were dispersed into 20 mL deionized water. Then, 0.01 M $NaBH_4$ deionized water solution was slowly added into the mixed solution until it became acidic. By filtering and washing thoroughly with deionized water, Pd NP/TiO_2 NB surface heterostructures were obtained. The contrast experiment of Pd deposit with and without TiO_2 nanobelts was also done. Without the TiO_2 nanobelts, the solution's color changed to brown, even black if the content of Pd was too much. But with TiO_2 nanobelts, the filtering solution was always without any color. This experiment proves that there was no homogeneous growth of separate Pd nanoparticles in the solution. This process was carried out at room temperature.

X-ray diffraction (XRD) patterns were recorded with a Bruker D8 Advance X-ray powder diffractometer with Cu Kα ($\lambda = 0.15406$ nm) radiation. Scanning electron microscopy (SEM) images obtained with a HITACHI S-4800 field emission scanning electron microscope and high-resolution transmission electron microscopy (TEM) images obtained with a JEOL JEM 2100 microscope were used to reveal the morphology and nanobelt/nanoparticle size of the synthesized samples. The Brunauer–Emmett–Teller (BET) surface areas were measured with a Builder 4200 instrument at liquid nitrogen temperature.

To test the gas sensing properties, the three kinds of nanobelt samples were coated onto the surface of cylindrical ceramic measurement tubes used to prepare gas sensors devices [14]. Fig 1a and b shows the schematic and actual picture of the gas sensor device along with the measuring circuit. 30 mg of sensing material was mixed with 0.5 mL of deionized water. After ultrasonic treatment for 10 min, the mixed slurry was divided into five equal portions, coated onto the outer surface of five ceramic tubes, and dried in air to obtain five sample devices for measurement. Two gold electrodes were soldered onto each end of each ceramic tube. A resistive heating wire was inserted into the ceramic tube for temperature control.

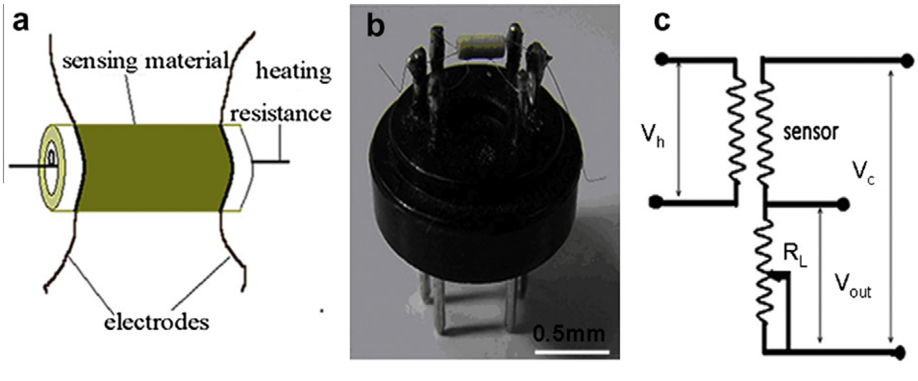

Fig. 1. (a) Schematic and (b) actual picture of the gas sensors; (c) schematic of the corresponding equivalent circuit.

Gas sensing measurements were carried out by using a static gas distribution method with a WS-30A gas sensing system (Zhengzhou Winson Electronics Technology Co. Ltd., P.R. China). The detailed procedure is described in Ref. [14]. Briefly, a fixed volume of liquid ethanol was injected onto a heating platform in the test chamber to prepare an ethanol-air gas mixture. As shown in Fig 1c, V_h is the heater voltage, V_c is the total voltage applied to the sensor resistance R and load resistance R_L in series, and V_{out} is the output voltage across R_L. The sensor resistance R can be determined using $R = R_L * (V_c - V_{out})/V_{out}$, and the sensitivity is defined as $S = R_a/R_g$, where R_a is the sensor resistance in air and R_g is the resistance when the sensor is exposed to the ethanol–air gas mixture. The humidity was controlled at about 30% during the measurements.

3. Results and discussion

Fig 2a displays the XRD pattern of the untreated TiO_2 nanobelts. The major peaks correspond to those of anatase titanium dioxide as listed in JCPDS file No. 21-1272. There are also some weak peaks corresponding to the TiO_2(B) phase as listed in JCPDS file No. 35-0088. The pattern indicates that the as-synthesized TiO_2 nanobelts are mainly anatase titanium dioxide with a small amount of TiO_2(B). Fig 2b is the XRD pattern for surface-coarsened TiO_2. All the peaks here correspond to anatase titanium dioxide with no detectable TiO_2(B) phase. In other word, the surface-coarsened TiO_2 consists of the anatase titanium dioxide phase only. The disappearance of TiO_2(B) likely results from corrosion by H_2SO_4 [39].

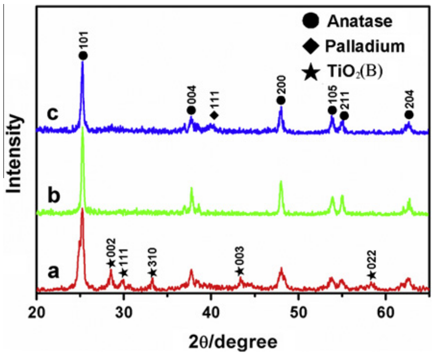

Fig. 2. XRD pattern of (a) TiO_2 nanobelts, (b) surface-coarsened TiO_2 nanobelts, and (c) Pd NP/TiO_2 NB surface heterostructures.

Fig 2c is the XRD pattern of the Pd NP/TiO_2 NB surface heterostructure. The main peaks correspond to anatase titanium dioxide and coincide with those of surface-coarsened TiO_2 shown in Fig 2b. Besides the anatase TiO_2 peaks, there is a very small peak corresponding to the (1 1 1) plane of Pd in JCPDS file No. 65-2867, which indicates that a small amount of elemental Pd particles are contained in the sample. The Pd content is much smaller than that of TiO_2 because the Pd peak is much weaker than that of anatase TiO_2. The size of the Pd particles is very small because of the very large half-width of the Pd (1 1 1) peak.

SEM and HRTEM were used to characterize the morphology of the sensing materials. Fig 3a and b are the SEM images for untreated TiO_2 nanobelts. From the images, one can see the as-synthesized TiO_2 is belt-structured, with a width of 50–200 nm, thickness of 20–40 nm, and length of several micrometers. The nanobelts have good flexibility and do not break even with winding and twisting, so the samples are very easy to handle in the experiments. Fig 3c and d are SEM images for surface-coarsened TiO_2. After an acid-assisted hydrothermal treatment with 0.02 M H_2SO_4 at 110 °C for 12 h, TiO_2 nanobelts retain their belt-like morphology without any appreciable change in width, thickness, or length. However, the surface of the TiO_2 nanobelts becomes coarsened by the attachment of a number of particles (of about 20 nm in diameter). These nanoparticles consist of TiO_2, the same phase as the nanobelts, according to the above XRD results. These results are in good agreement with our previous work [1,24,25]. What is more, the surface-to volume ratio also increases from 26.7453 m^3/g of TiO_2 nanobelts to 46.6357 m^3/g of surface-coarsened TiO_2 nanobelts.

Fig. 3e–h show HRTEM images for Pd NP/TiO_2 NB surface heterostructures. As shown in Fig 3e and f, the numerous dots are uniformly distributed on the as-synthesized nanobelts. These dots are about 3–5 nm in diameter, as shown in Fig 3g. They are Pd nanoparticles, according to the XRD results and Fig 3h. In addition, it should be noted that the Pd nanoparticles are firmly attached to the TiO_2 nanobelt surface to form a heterostruture. The junction between the Pd nanoparticles and the nanobelts remains intact even after ultrasonic treatment for 30 min. As well known, TiO_2 nanoparticles is negatively charged, and Pd cations are positive ions. When the TiO_2 nanobelts immerse into the $PdCl_2$ solution, some platinum ions absorbed on the surface of the nanobelts and form local high concentration area. When the $NaBH_4$ was dropped into the solution, the reduction occurs in such area and the nuclei form on surface of the nanobelt. With the reduction process continues, Pd nuclei grow to be nanoparticles on the surface of TiO_2 nanobelts and form uniformly distributed surface heterostruc-

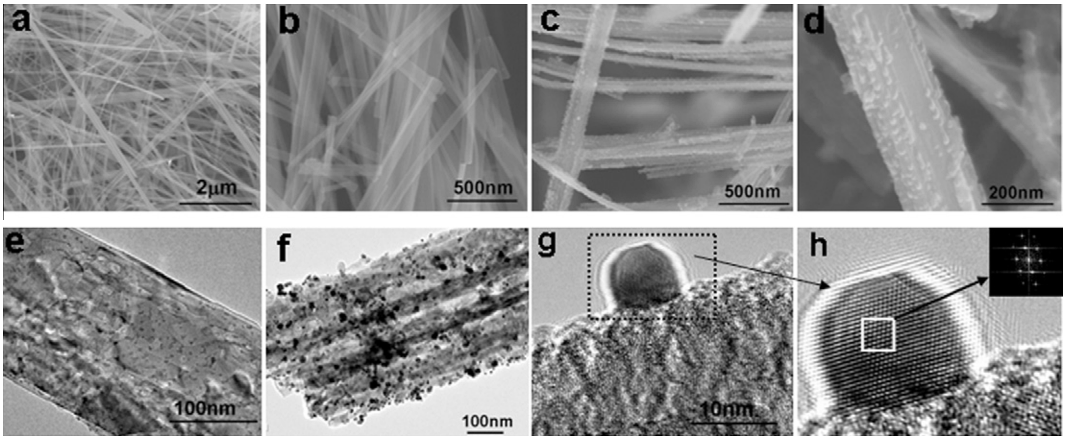

Fig. 3. SEM image of (a and b) TiO_2 nanobelts and (c and d) surface-coarsened TiO_2 nanobelts; (e–h) HRTEM image of Pd NP/TiO_2 NB surface heterostructures.

tures. Because of the pinning effect of the nanoparticle caused by the nano-junction, the Pd nanoparticle cannot move and aggregate during the filter process. The heterostructure containing the Pd nanoparticles and the TiO_2 nanobelts forms Schottky barrier-type junctions, because the Pd nanoparticles are metallic, and the TiO_2 nanobelts are semiconductors, thus greatly enhancing the gas sensitivity for oxides [34].

The ethanol vapor sensing performance of the nanobelts obtained above was measured by using the static gas distribution method detailed in Ref. [14]. Briefly, a fixed volume of liquid ethanol was injected onto a heating platform in the test chamber to prepare an ethanol–air gas mixture. In order to determine the best working temperature, the sensitivity of the samples prepared with the three kinds of nanobelt material, TiO_2 nanobelts, surface-coarsened TiO_2 nanobelts, and Pd NP/TiO_2 NB surface heterostructures was measured upon exposure to an ethanol–air vapor mixture with an ethanol concentration of 500 ppm at different temperatures, As shown in Fig 4a, the sensors based on TiO_2 nanobelts exhibit very low sensitivity at room temperature. The sensitivity increases with increasing temperature, reaches a maximum at 200 °C, at a value of 4.84, and decreases with further temperature increase. Although the variation of gas sensitivity on temperature for sensors based on surface-coarsened TiO_2 nanobelts is the same as that for TiO_2 nanobelts, after surface coarsening, the sensitivity increases much more rapidly, reaches a peak value and decreases much more rapidly with increasing temperature. The sensitivity is 17.22 for surface-coarsened TiO_2 nanobelts at 200 °C, which is more than three times the sensitivity of TiO_2 nanobelts without surface coarsening. The sensitivity of the sensor based on Pd NP/TiO_2 NB surface heterostructures shows the strongest temperature dependence while sharing the same sensitivity vs temperature trend. As shown in Fig 4a, the sensitivity values of this sample are much higher than those of the other two samples at all measurement temperatures. The optimal sensing temperature is also 200 °C with a highest sensitivity value of 48.84, 3 times that of the surface-coarsened TiO_2 nanobelt sensors, and 10 times that of TiO_2 nanobelts without any treatment. The above results demonstrate that surface-coarsening improves the ethanol sensitivity of TiO_2 nanobelts, and that the Pd/TiO_2 junctions enhance the gas sensitivity dramatically. As mentioned above, the best working temperature for the Pd NP/TiO_2 NB surface heterostructure is 200 °C, which is quite low compared with other materials reported in the literature [20,22,25,27,34,40].

To optimize the Pd content and hereby obtain the best sensor material, the sensitivity of Pd NP/TiO_2 NB surface heterostructures with different Pd loading was measured at different ethanol concentration at the optimal working temperature of 200 °C. The gas sensitivity of Pd NP/TiO_2 NB surface heterostructures with different Pd content are shown in Fig 4b. While the concentration of ethanol is fixed at 10 ppm, the sensitivity increases with increasing Pd concentration up to 4 wt.%, reaching a maximum at that point, and then dropping off when the Pd content is increased beyond 4 wt.%. This result reveals that a small amount of Pd is sufficient to enhance the gas sensitivity of the TiO_2 nanobelts. As the ethanol concentration is increased from 10 ppm to 500 ppm, the trend is similar to that obtained with 10 ppm. With a lower Pd content, the enhancement of the gas sensitivity can be attributed to the nanoscopic depletion region (nano-Schottky barriers) surrounding the Pd nanoparticle, which reduces the nanobelt conductance through electron transfer from the nanobelt to Pd nanoparticle. The subsequent decrease when the Pd content exceeds 4 wt.% is possibly caused by the overlap between neighboring Pd particles

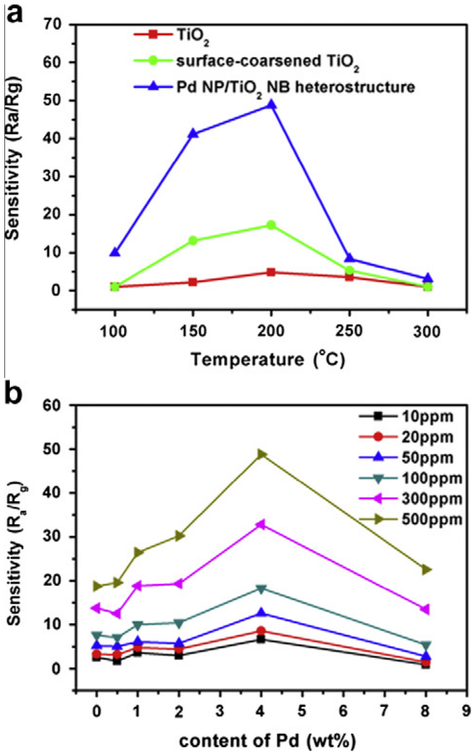

Fig. 4. (a) Sensitivity with 500 ppm ethanol vapor at different temperatures, (b) sensitivity profiles of ethanol vapor sensor based on Pd NP/TiO_2 NB surface heterostructures with different Pd content at 200 °C.

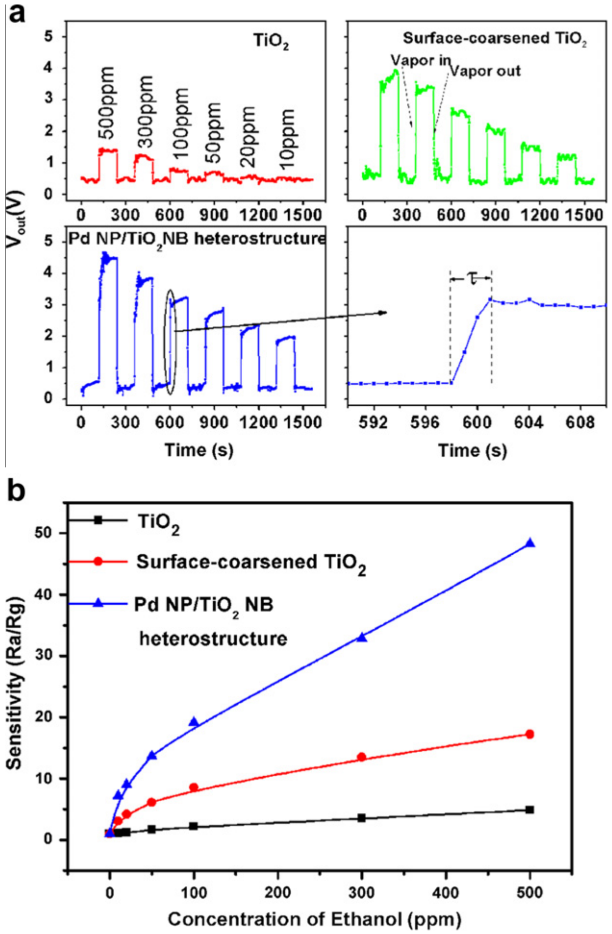

Fig. 5. (a) Response curve and (b) sensitivity profile of sensors upon exposure to different concentrations of ethanol vapor at 200 °C.

[34], and as a result, the surface area of the TiO_2 nanobelt that is exposed to air is decreased, indicating that TiO_2 is the key component in gas sensing.

Based on the above measurements, TiO_2 nanobelts, surface-coarsened TiO_2 nanobelts, and Pd NP/TiO_2 NB surface heterostructures with 4 wt.% Pd were selected as sensing materials. Fig 5 shows the behavior of sensors based on the three kinds of material at a working temperature of 200 °C. In our experiment, sensors based on TiO_2 nanobelts, surface-coarsened TiO_2 nanobelts and Pd NP/TiO_2 NB surface heterostructures were exposed to an ethanol–air gas mixture at 200 °C with a concentration of 500 ppm, 300 ppm, 100 ppm, 50 ppm, 20 ppm, and 10 ppm ethanol in that order. The value of V_{out} increases remarkably as the concentration of ethanol increases from 10 ppm to 500 ppm. It should be noted that the minimum detectable concentration of ethanol for the sensor based on TiO_2 nanobelts with no treatment is 50 ppm (upper-left in Fig 5a), whereas for the sensors based on the other two materials, an apparent response to ethanol vapor at 10 ppm (upper-right in Fig 5a for surface-coarsened TiO_2 nanobelts and lower-left in Fig 5a for Pd NP/TiO_2 NB surface heterostructures) is exhibited. Most importantly, the response/recovery time for the both samples is about 4 s (as shown in the lower-right of Fig 5a), which is at least 10 times shorter than the value for sensors based on Pd–SnO_2 [34] and ZnO [40], and even 800 times shorter than that of Pd-carbon nanotube sensors [37]. In Fig 5b, the sensitivity profile of the sensors upon exposure to different concentrations of ethanol vapor at 200 °C is displayed. The profile resembles half of a hyperbola and varies almost linearly with the ethanol concentration at high concentrations (more than 50 ppm). The sensitivity (taking the average of five similar sensors) based on TiO_2 nanobelts, surface-coarsened TiO_2 nanobelts, and Pd NP/TiO_2 NB surface heterostructures increases from 1.06, 3.07, and 7.16, respectively, at 10 ppm ethanol vapor to 4.84, 17.22, and 48.83, respectively, at 500 ppm ethanol vapor. All in all, the sensitivity increases in the order: TiO_2 nanobelts < surface-coarsened TiO_2 nanobelts < Pd NP/TiO_2 NB surface heterostructures, confirming the enhancement effects of surface-coarsening and functionalization with Pd catalyst particles onto the TiO_2 nanobelts.

In order to examine stability and reproducibility, the sensors based on TiO_2 nanobelts, surface-coarsened TiO_2 nanobelts, and Pd NP/TiO_2 NB surface heterostructures were exposed to 500 ppm ethanol vapor at 200 °C at a minimum of three times. Fig 6 displays the response curves. For all three kinds of sensor, as soon as the ethanol vapor was introduced into the chamber, the value of V_{out} increased immediately and reached the higher stable value within 4 s. When the ethanol vapor was exhausted from the chamber, the value of V_{out} recovered to its original value immediately. The response of the sensors was almost the same each time and could be reproduced even after exposing the samples to air at room temperature for several months. Fig. 6d shows another experiment of Pd NP/TiO_2 NB surface heterostructure, and the sensitivities for ethanol of 10 ppm, 20 ppm, 50 ppm, 100 ppm, 300 ppm, and 500 ppm are 3.34, 9.82, 14.54, 20.31, 34.01, and 50.02, respectively. This is almost the same as the original ones. All the above results demonstrate the stability and reproducibility of the sensors.

Selectivity is another important property for gas sensors. To measure the selectivity of the sensors based on Pd NP/TiO_2 NB surface heterostructures, they were exposed to other vapors/gases, including CH_3COCH_3, CO, H_2, and CH_4. Fig 7 displays the response curves of sensors based on Pd NP/TiO_2 NB surface heterostructures upon exposure to different vapors/gases at 200 °C. It was found that the sensors were insensitive to CH_4 and showed a much lower response to CO, H_2, and CH_3COCH_3 than to ethanol at 200 °C. The sensitivity for 500 ppm CO, H_2, CH_3COCH_3 and CH_3CH_2OH is 4.94, 5.96, 17.55, and 48.83, respectively. Clearly, sensors based on Pd NP/TiO_2 NB surface heterostructures exhibit excellent selectivity. According to the above results, the ethanol vapor sensor based on Pd NP/TiO_2 NB surface heterostructures exhibits the best sensitivity, selectivity, working temperature, response/recovery time, and reproducibility.

The sensing mechanism of the TiO_2 nanobelts can be explained using a surface-depletion model [14,34]. Similar to other sensors based on oxide semiconductors, the gas sensing mechanism of TiO_2 is based on the change in resistance when exposed to different gases. As is well known, there are no free electrons in TiO_2 nano-

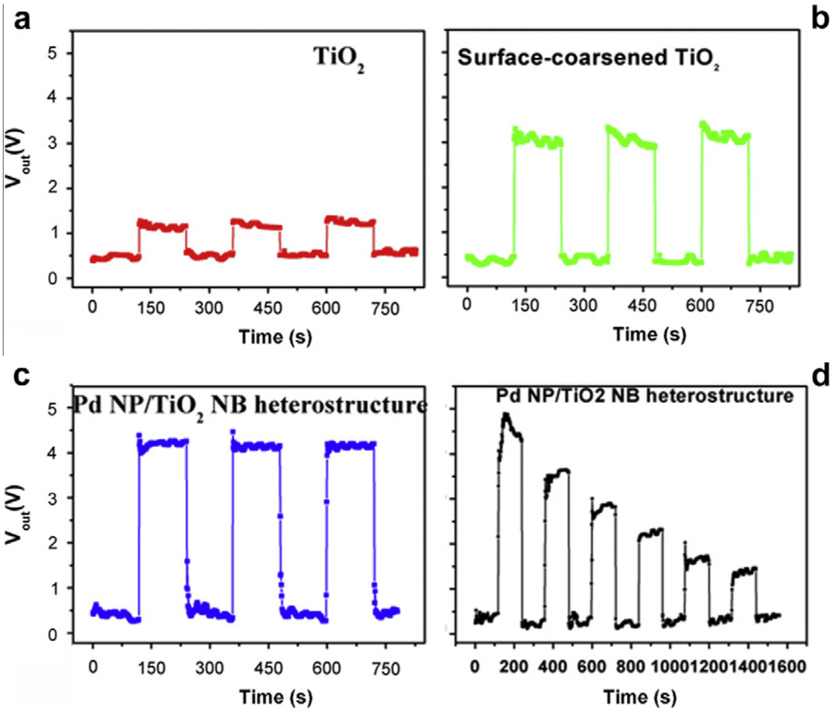

Fig. 6. Response curve upon exposure to 500 ppm ethanol vapor at 200 °C 3 times.

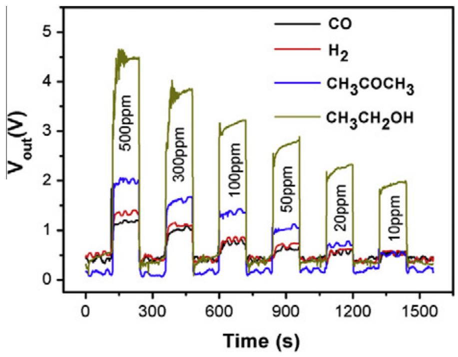

Fig. 7. Response curve of sensors based on Pd NP/TiO_2 NB surface heterostructures upon exposure to different gases or vapors at 200 °C.

belts at absolute zero (−273.15 °C), while at the working temperature (200 °C), some electrons (only a few) are excited, having transferred from the valence band to the conduction band and becoming free electrons, which induces the nanobelt to become weakly conducting. When the sensors are exposed to air, an oxidizing gas (e.g., O_2) is adsorbed onto the TiO_2 surface, and the adsorbed O_2 will combine with the electrons from the TiO_2 conduction band [14], resulting in a surface charge depletion layer, and to some extent an increase in the resistance of the nanobelt surface. Due to the small thickness of the nanobelt, the surface charge depletion layer almost spans the entire width of the belt and the resistance change of the belt is essentially the same as that of the surface. When the sensor is exposed to a reducing gas (e.g., CH_3CH_2OH), electron transfer occurs from CH_3CH_2OH to TiO_2, and the adsorbed O_2 acts as an "electron bridge" in this case (Fig. 8a). This electron transfer leads to a resistance decrease in the TiO_2 nanobelt, thus explaining the enhancement of V_{out} in our experiments.

Based on the above theory, through a surface-coarsening treatment, the surface-to-volume ratio increases and there are more surface defects and thus more active crystal planes exposed to the air. The surface defects serve as adsorption centers for O_2 and CH_3CH_2OH (Fig. 8b), and the active layers speed up the reaction between O_2 and ethanol vapor. All of the above mechanisms enhance the sensitivity of the nanobelts.

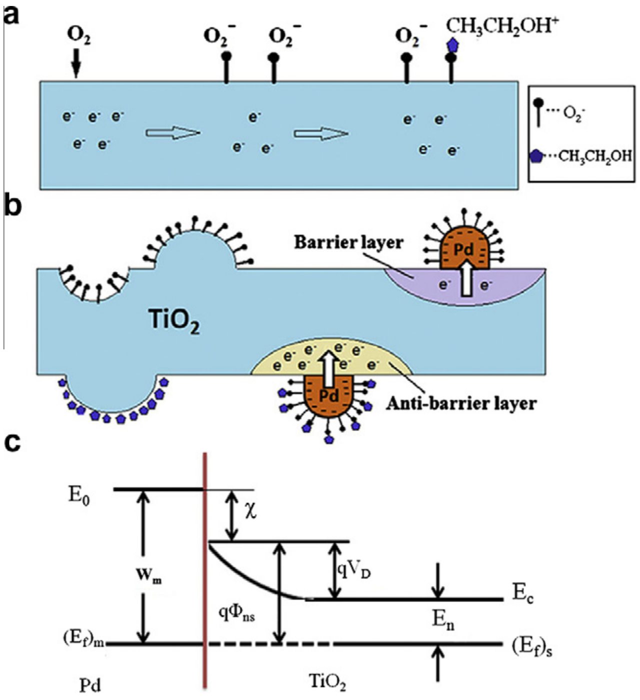

Fig. 8. Sensing mechanism of TiO_2 nanobelts to ethanol.

The nano-Schottky barrier formed by the functionalization of TiO_2 nanobelts with Pd particles can be used to explain the enhancement of the gas sensitivity^{34}. The work function of Pd and TiO_2 is 5.12 eV and 4.2 eV, respectively, as shown in Fig. 8c. Here, W_m is the work function of Pd, $(E_f)_m$ is the fermi level of Pd, $(E_f)_s$ is the fermi level of TiO_2, E_c is the conduction band level, E_n is half of the band gap of TiO_2, the barrier height of Pd is $q\varphi_{ns} = W_m - \chi$, and barrier height of TiO_2 is $qV_D = W_m - W_s$, here χ is the Fermi level change of TiO_2 when contacts Pd, q is the charge of electrons, W_s is the work function of TiO_2. When they contact each other, electrons are transferred from the TiO_2 nanobelt to the Pd nanoparticles (Fig. 8b), forming a barrier layer (an area with high resistance) around the Pd nanoparticles, and so the Pd nanoparticle becomes an accumulation area for electrons, forming an electronegative surface. When O_2 molecules adsorb onto the surface, they accumulate on the surface of the Pd particles. Then when the nanobelts are exposed to ethanol vapor, the Pd particles serve as an ethanol sink. Electron transfer thus occurs from CH_3CH_2OH to the Pd nanoparticles and then to the TiO_2 nanobelt. Because of the existence of the electron-rich Pd nanoparticles, electron transfer can be realized much more easily. As a result, the "barrier layer" is transformed into an "anti-barrier layer" (an area with high conductance) [41]. Given their small thickness, the barrier layer or anti-barrier layer can influence the total conductance of the nanobelt, which brings about a great enhancement in sensitivity. However, at higher temperatures, ethanol and oxygen do not adsorb well onto the solid surface, and so the electron transfer across the interface becomes much less active; also, there are more free electrons in the nanobelt, and the transferred electrons are much fewer in number compared with the number of free electrons in the nanobelt. So, when the TiO_2 nanobelt is exposed to air, few electrons are trapped by the adsorbed O_2, but there are also quite a lot of electrons in the nanobelt. This causes a smaller resistance change in the nanobelt, which as a result exhibits low sensitivity. This mechanism explains the decrease in sensitivity at temperatures over 200 °C.

4. Conclusion

TiO_2 nanobelts, surface-coarsened TiO_2 nanobelts, and Pd NP/TiO_2 NB surface heterostructures were successfully synthesized through hyrothermal, acid corrosion, and precipitation–reduction methods. The nanobelts were fabricated with a width of 50–200 nm, a thickness of 20 nm, and a length of several micrometers, and the functionalized Pd nanoparticles on the surface were 3–5 nm in diameter.

Gas sensing measurements on these three kinds of material proved that they all possess good ethanol sensitivity. The sensors based on Pd NP/TiO_2 NB surface heterostructure nanobelts exhibit the best performance, including the highest sensitivity and selectivity, lower working temperature, and good reproducibility.

The sensing mechanism can be explained using a surface-depletion model and positing a nano-Schottky barrier between the Pd nanoparticle and the TiO_2 nanobelt. These materials exhibit excellent ethanol detection properties and have great promise in applications requiring ethanol detection for transportation safety and in the alcohol manufacturing industry.

Acknowledgments

This research was supported by NSFC (NSFDYS: 50925205, 50872070, 60974117, 51002089). And the Program of Introducing

Talents of Discipline to Universities in China (111 program No. b06015), Independent Innovation Foundation of Shandong University (2010JQ004), Shandong Provincial Natural Science Foundation, China (JQ201117).

References

[1] J. Joo, S.G. Kwon, T. Yu, M. Cho, J. Lee, J. Yoon, T. Hyeon, J. Phys. Chem. B 109 (32) (2005) 15297–15302.
[2] G.K. Mor, K. Shanker, M. Paulose, O.K. Varghese, C.A. Grimes, Nano Lett. 6 (2) (2006) 215–218.
[3] S. Takabayashi, R. Nakamura, Y. Nakato, J. Photochem. Photobiol. A 166 (2004) 107–113.
[4] C.R. Sides, C.R. Martin, Adv. Mater. 17 (1) (2005) 125–128.
[5] A. Zak, Y. Feldman, V. Lyakhovitskaya, G. Leitus, R. Popovitz-Biro, E. Wachtel, H. Cohen, S. Reich, R. Tenne, J. Am. Chem. Soc. 124 (17) (2002) 4747–4758.
[6] W. Sugimoto, O. Terabayashi, Y. Murakami, Y. Takasu, J. Mater. Chem. 12 (2002) 3814.
[7] G.Z. Cao, J. Phys. Chem. B 108 (52) (2004) 19921–19931.
[8] D.V. Bavykin, A.A. Lapkin, P.K. Plucinski, J.M. Friedrich, F.C. Walsh, J. Phys. Chem. B 109 (41) (2005) 19422–19427.
[9] S.H. Lim, J.Z. Luo, Z.Y. Zhong, W. Ji, J.Y. Lin, Inorg. Chem. 44 (12) (2005) 4124–4126.
[10] M. Gratzel, J. Photochem. Photobiol. C 4 (2) (2003) 145.
[11] C.G. Granqvist, Adv. Mater. 15 (21) (2003) 1789–1803.
[12] W.J. Dong, T.R. Zhang, J. Epstein, L. Cooney, H. Wang, Y.B. Li, Y.B. Jiang, A. Cogbill, V. Varadan, Z.R. Tian, Chem. Mater. 19 (18) (2007) 4454–4459.
[13] X. Chen, S.S. Mao, Chem. Rev. 38 (41) (2007) 2891–2959.
[14] P.G. Hu, G.J. Du, W.J. Zhou, ACS Appl. Mater. Interface 2 (11) (2010) 3263–3269.
[15] W. Zhou, H. Liu, R.I. Boughton, G. Du, J. Lin, J. Wang, D. Liu, J. Mater. Chem. 20 (2010) 5993–6008.
[16] Y. Xia, P. Yang, Y. Sun, Y. Wu, B. Mayers, B. Gates, Y. Yin, F. Kim, H. Yan, Adv. Mater. 15 (5) (2003) 353–389.
[17] G. Pan, P. He, Y. Sun, J. Cao, J. Mater. Sci. Eng. 6 (2007) 965–968.
[18] A. Kolmakov, Y. Zhang, G. Cheng, M. Moskovits, Adv. Mater. 15 (12) (2003) 997–1000.
[19] M. Li, Y. Chen, Sens. Actuators A 32 (1) (1996) 83–85.
[20] L. Francioso, D.S. Presicce, A.M. Taurino, R. Rella, P. Siciliano, A. Ficarella, Sens. Actuators, A 95 (1–3) (2003) 66–72.
[21] M. Ferroni, V. Guidi, G. Martinelli, G. Faglia, P. Nelli, G. Sherveglieri, Nanostructured Mater. 7 (7) (1996) 709–718.
[22] L.R. Skubal, N.K. Meshkov, M.C. Vogt, J. Photochem. Photobiol. A 148 (1–3) (2002) 103.
[23] Q. Zheng, B. Zhou, J. Bai, L. Li, Z. Jin, J. Zhang, J. Lin, Y. Liu, W. Cai, X. Zhu, Adv. Mater. 20 (5) (2008) 1044–1049.
[24] H. Lin, C. Keng, C. Tung, Mater. Charact. 58 (8–9) (2007) 680–684.
[25] C. Garzella, E. Comini, E. Tempesi, C. Frigeri, G. Sberveglieri, Sens. Actuators, A 68 (1–3) (2000) 189196.
[26] L. Francioso, A.M. Taurino, A. Forleo, P. Siciliano, Sens. Actuators, A 130 (1) (2008) 70–76.
[27] A.M. Ruiz, G. Sakai, A. Cornet, K. Shimanoe, J.R. Morante, N. Yamazoe, Sens. Actuators, A 93 (1–3) (2003) 509–518.
[28] R.K. Sharma, M.C. Bhatnagar, G.L. Sharma, Appl. Surf. Sci. 92 (1996) 647–650.
[29] K. Zakrzewska, Vacuum 74 (2) (2004) 335–338.
[30] R.K. Sharma, M.C. Bhatnagar, G.L. Sharma, Sens. Actuators, A 45 (3) (1997) 209–215.
[31] D. Morris, R.G. Egdell, J. Mater. Chem. 11 (2011) 3207–3210.
[32] E. Traversa, M.L.D. Vona, S. Licoccia, J. Sol–Gel Sci. Technol. 22 (1–2) (2001) 167–179.
[33] X. Du, Y. Wang, Y. Mu, L. Cui, P. Wang, Y. Tang, Chem. Mater. 14 (9) (2002) 3953–3957.
[34] A. Kolmakov, D.O. Klenov, Y. Lilach, S. Stemmer, M. Moskovits, Nano Lett. 5 (4) (2005) 667–673.
[35] S. Bao, C. Li, J. Zang, X. Cui, Y. Qiao, J. Guo, Funct. Mater. 18 (4) (2008) 591–599.
[36] R. Wu, Y. Sun, C. Lin, H. Chen, M. Chavali, Sens. Actuators, A 115 (1) (2006) 198–204.
[37] P. Jain, D.A. Fonseca, E. Schaible, A.D. Lueking, J. Phys. Chem. C 111 (4) (2007) 1788–1800.
[38] Y. Wang, G. Du, H. Liu, D. Liu, S. Qin, N. Wang, C. Hu, X. Tao, J. Jiao, J. Wang, Z. Wang, Adv. Funct. Mater. 18 (7) (2008) 11311137.
[39] W.J. Zhou, L.G. Gai, P.G. Hu, J.J. Cui, X.Y. Liu, D.Z. Wang, G.H. Li, H.D. Jiang, D. Liu, H. Liu, J.Y. Wang, CrystEngComm 13 (2011) 6643–6649.
[40] H. Xu, X. Liu, D. Cui, M. LI, M. Jiang, Sens. Actuators, A 114 (1) (2006) 301–307.
[41] E. Liu, B. Zhu, J. Luo, Semiconductor Physics, forth ed., National Defense Industry Press, Beijing, 2007.